Solar Energy Materials & Solar Cells 149 (2016) 103–109

Contents lists available at ScienceDirect

Solar Energy Materials & Solar Cells

journal homepage: www.elsevier.com/locate/solmat

Fully roll-to-roll prepared organic solar cells in normal geometry with a sputter-coated aluminium top-electrode

Thomas R. Andersen [a,*], Nathan A. Cooling [a], Furqan Almyahi [a,b], Andrew S. Hart [a], Nicolas C. Nicolaidis [a], Krishna Feron [a,c], Mahir Noori [a,d], Ben Vaughan [a,c], Matthew J. Griffith [a], Warwick J. Belcher [a], Paul C. Dastoor [a]

[a] Centre for Organic Electronics, University of Newcastle, University Drive, Callaghan, NSW 2308, Australia
[b] Department of Physics, College of Science, University of Basrah, Iraq
[c] CSIRO Energy Technology, Newcastle, NSW 2300, Australia
[d] Department of Physics, College of Education for Pure Science, University of Anbar, Iraq

ARTICLE INFO

Article history:
Received 28 October 2015
Received in revised form
7 December 2015
Accepted 12 January 2016

Keywords:
Roll-to-roll processing
Sputter coating
Normal geometry
Organic photovoltaics
Printing

ABSTRACT

We demonstrate a pathway for fully roll-to-roll (R2R) prepared organic solar cells in a normal geometry with a R2R sputtered aluminium top electrode. Initial attempts utilizing a stack geometry without an electron transport layer (ETL) failed to obtain working devices. By applying aluminium zinc oxide (AZO) as an ETL, and optimizing the AZO thickness, working printed OPV devices with an efficiency of 0.58% were obtained. Further optimization of the donor:acceptor ratio in the active layer increased the efficiency to 0.90%. This work demonstrates that normal geometry organic solar cells using a metal top contact can be produced using large scale production techniques.

1. Introduction

Solution-processed bulk heterojunction organic solar cells (OSCs) have received much interest from the research community during the last couple of decades due to their enormous potential as a low cost energy source [1,2]. The key-advantage of OSCs compared to conventional solar cells technologies is the capability of the materials to be solution processed by high throughput roll-to-roll (R2R) processing techniques; other advantages include low temperature processing and flexible substrates [3,4]. Even though the efficiency for small area (<0.1 cm^2) devices has increased from approximately 2.5% in 2001 to 11.0% in 2014 [5], and that it is well-known that R2R techniques must be utilized for cost-effective fabrication of OSCs, only a few groups have turned their focus towards upscaling. Fabrication of large scale OSCs by R2R processing presents the unique challenge of generating uniform thin films with tailored morphologies and interfaces over stretches of hundreds of metres. By contrast, most laboratory scale OSCs are prepared by spin coating with an active area of <10 mm^2 on a rigid glass substrate with indium tin oxide (ITO) as the transparent electrode [6]. Large scale production of OSCs uses a range of coating and printing techniques for ink deposition such as slot-die coating, flexographic printing and rotary screen printing [7,8]. Flexible substrates with a printed silver and coated poly(3,4-ethylenedioxythiophene) polystyrene sulfonate (PEDOT:PSS) electrode are commonly utilized for large scale OSC production to avoid the use of scarce materials such as indium [9,10]. The silver PEDOT:PSS electrode combination has been reported to obtain sheet resistance of 10.4 Ω/□ and is therefore comparable to ITO [9]. The most impressive OSC upscaling work to date was conducted by Krebs et al. [4] who produced a stretch of 21,000 defect free cells connected in series. This array of OSCs yielded over 10 kV under illumination with an overall performance of 1.5%.

The bulk of published work in the area of large scale OSCs prepared using R2R techniques has utilized inverted structure devices with a silver top electrode [9,11–14]. This structure represents a deviation in device geometry compared to laboratory scale devices, which typically have an evaporated electrode [6]; creating extra challenges on top of the already difficult process of upscaling [15]. Previous attempts to prepare normal geometry solar cells via R2R coating and printing techniques have all been with a non-scalable top electrode deposited by thermal evaporation [16–18]. Recently, Griffith et al. reported a procedure for sputter coating an aluminium top electrode onto OSCs [19]. In contrast to thermal evaporation, sputter coating is a widely used

* Corresponding author.
E-mail address: thomas.andersen@newcastle.edu.au (T.R. Andersen).

http://dx.doi.org/10.1016/j.solmat.2016.01.012
0927-0248/

technique for the deposition of metal thin films on an industrial scale. There are three main advantages of a sputtered electrode over a printed silver electrode: 1) The sputtered back electrode is a reflective surface, allowing the preparation of thinner active layers whilst maintaining optical absorption, 2) OSC devices prepared in normal geometry exhibit enhanced V_{OC}'s compared inverted geometry devices [20–22], 3) The harsh solvents and mechanical force present when flexographically printing or screen coating a top silver contact (which can lead to penetration of silver and solvent through previously coated layers to form areas with no photocurrent extraction [14,23]) are eliminated.

In this work we show the preparation and active layer optimization of flexible ITO-free organic solar cells by R2R coating and printing techniques using a R2R sputter-coated aluminium top electrode. This work demonstrates, for the first time, that normal geometry OSCs using a metal top contact can be produced using R2R techniques suited to large scale production.

2. Results and discussion

2.1. Device architecture optimization

Initial studies were conducted using cells with device geometry Structure A from Fig. 1 without an electron transport layer (ETL) as described in the literature [19] and with an active layer thickness of 500 nm. The active layer thickness was chosen to ensure that silver spikes found on the height profile in Fig. 1 were embedded in the active layer. The silver spikes had a height of approximately 250 nm, but larger spikes with a height of up to 350 nm were also present. Similar silver spikes have previously been observed on similar silver grid/PEDOT:PSS electrodes [24]. The prepared devices did, however, exhibit only limited solar cell characteristics as seen in Fig. 2; the obtained *J–V* curve has a slight S-shape with a FF of 23% and the J_{SC} is only 0.04 mA cm^{-2}. It has been suggested that the sputtering of metal onto soft organic layers can cause deep penetration of the metal due to the higher energy nature of sputtering as compared to thermal evaporation [25–27]. This phenomenon has been thought to cause shorts between the contacts in OSCs when sputtering has been employed for the top electrode. However, work by Griffith et al. has shown that, rather than causing deep penetration, the sputtering of aluminium on organic films forms an oxide layer near the active layer/sputtered electrode interface unless careful processing measures are undertaken [19]. This oxide layer can have a detrimental effect on the performance of the OSC device.

In an attempt to overcome this issue, Structure B was utilized where an AZO layer was added as an ETL between the active layer and the sputtered aluminium electrode. AZO was chosen since it is a hard inorganic material (decreasing the likelihood of sputtering damaging the active layer) and no photoactivation is required, as is the case for example zinc oxide [28]. It was postulated that any residual oxygen present during the sputtering process should interact with the AZO layer rather than forming an oxide within the active layer. This hypothesis is supported by the *J–V* curves of devices containing an AZO layer as an ETL, which exhibit the desired J-shape (Fig. 2A) and a J_{SC} of 0.2 mA cm^{-2}, V_{OC} of 0.39 V

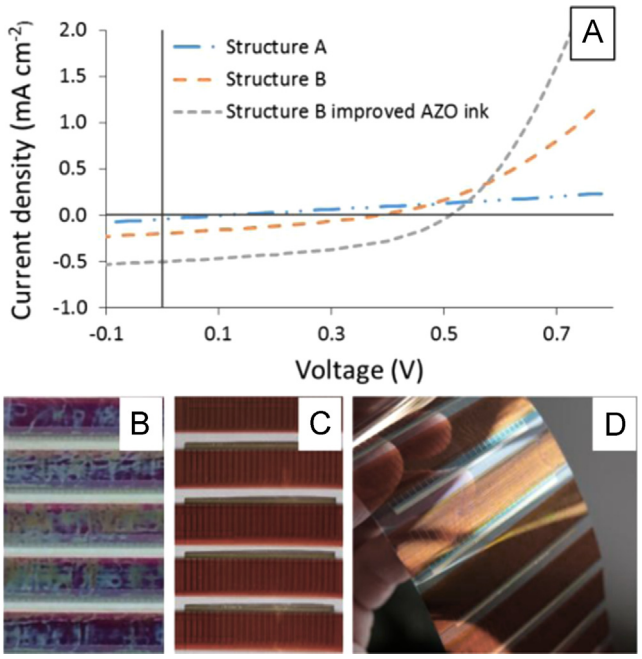

Fig. 2. (A) *J–V* characteristics of devices prepared with device Structure A, Structure B and Structure B with improved AZO ink, (B) Picture presentation of AZO layers prepared from a pure methanol AZO ink coated on top of active layer, (C) Picture of layer stack with optimized methanol:IPA AZO ink coated on top of active layer, and (D) Layer stack from picture B presented with light reflection. (For interpretation of the references to colour in this figure, the reader is referred to the web version of this article.)

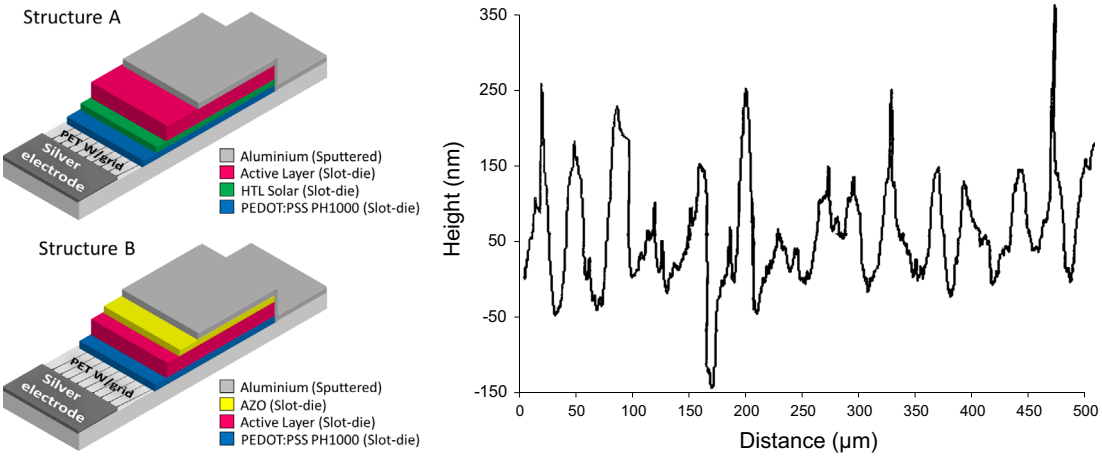

Fig. 1. Left: Two device structures were employed during the work presented in this paper along with deposition methods for the individual layers. Both device structures are in normal geometry but Structure A contains PEDOT:PSS as a hole transport (HTL) layer whereas Structure B contains aluminium doped zinc oxide (AZO) as an ETL layer. Right: Height profile of the silver PEDOT:PSS electrode along one of the silver fingers.

and FF of 32.2%; representing an increase in all photovoltaic parameters in comparison with devices prepared with Structure A.

The initial AZO films coated with a methanol based ink formulation were of poor quality, as seen in Fig. 2B. Prior to coating the AZO film the active layer was pre-wet with isopropanol (IPA), which was found to promote wetting. However, during drying an inhomogeneous layer formed, which was likely due to the poor compatibility between the active layer and the AZO ink. IPA is a commonly used solvent for improving the wettability of PEDOT:PSS [24,29] on active layer, and given that PEDOT:PSS is a water based suspension, it was speculated that IPA should have a similar beneficial effect on the wettability of the AZO methanol based ink. Indeed, the AZO film quality was significantly improved by utilizing a 65:35 mixture of AZO ink and IPA, respectively, as pictured in Fig. 2C and D where only a very little colour change across the stripe is observed in the AZO film. Moreover, the efficiency of the OSC devices improved from 0.02% to 0.12% with the improvement in film quality of the AZO layer.

2.2. Active layer thickness optimization

Device optimization was conducted based on the work by Dibb et al. [30] and Andersen et al. [24], which showed that a reduction in the active layer thickness from 330 nm and 480 nm to 200 nm results in OSC devices with significantly improved J_{SC} when illuminating through the anode. The thickness of the active layer was optimized by preparing five types of devices, each with a different thickness varying from 500 nm to 150 nm. As seen in Fig. 3, the J_{SC} is increased significantly (from 0.52 to 2.20 mA cm^{-2}) by reducing the thickness from 500 to 200 nm. Preparation of devices with an active layer thinner than 200 nm was not feasible due to critical failure during switching (Fig. 6) and therefore 200 nm was found to be the lower thickness limit for the active layer when applying an active layer with a 1:1 ratio between the P3HT donor and the ICxA acceptor. The increase in J_{SC} with a thinner active layer clearly indicates that the short circuit current density limitation is not a consequence of a lack of light absorption. This increase in J_{SC} as the active layer thickness reduces also highlights the advantage of using a reflective back electrode in improving optical absorption. The lower J_{SC} in the thicker active layer devices could be due to either the active layer having isolated areas of donor and acceptor or charge carrier transport limitations of the active layer. Both possibilities would lead to a loss of charge carriers as a consequence of recombination [31–33]. The loss of charge carriers due to increased active layer film thickness is also evident in the EQE data presented in Fig. 3B, particularly the devices prepared with film thicknesses of 500 and 375 nm. These two devices show a significant dip in EQE around 475 nm which is approximately where P3HT has its maximum absorption [34].

2.3. Active layer ratio optimization

Regardless of whether the J_{SC} is reduced due to isolated domains or poor charge carrier transport, one method to potentially overcome these issues is to vary the donor:acceptor ratio to optimize the film morphology i.e. crystallinity and domain sizes. Such alterations have been seen previously for similar materials when their ratio has been changed [35]. In the current work, device switching was significantly affected by the active layer ratio. Active layers down to 150 nm in thickness were able to be switched if the donor:acceptor ratio was changed from the initial 1:1 P3HT:ICxA ratio to a 5:4 or 3:2 P3HT:ICxA ratio, whereas an active layer using a ratio of 2:3 P3HT:ICxA could only be switched down to an active layer thickness of 250 nm. Furthermore, even at an active layer thickness of 250 nm, the device could not be completely switched as evidenced by the *I–V* curve in Fig. 4A where a significantly reduced open circuit voltage of 0.48 V was observed for the 2:3 ratio, and the prepared OSC devices exhibited poor photovoltaic characteristics. Devices prepared with the increased P3HT fraction had a higher performance than that observed for the 1:1 ratio devices; resulting from an increased J_{SC} from 2.20 to 2.80 mA cm^{-2}. This trend was also reproduced in the EQE data in Fig. 4. The devices also exhibited a minor increase in FF from 43% to 49%, which is a clear indication of improved transport through the device since a larger J_{SC} would be expected to reduce the FF [36,37].

Laser beam induced current (LBIC) images (Fig. 5) reveal the presence of fine horizontal lines in the prepared devices from

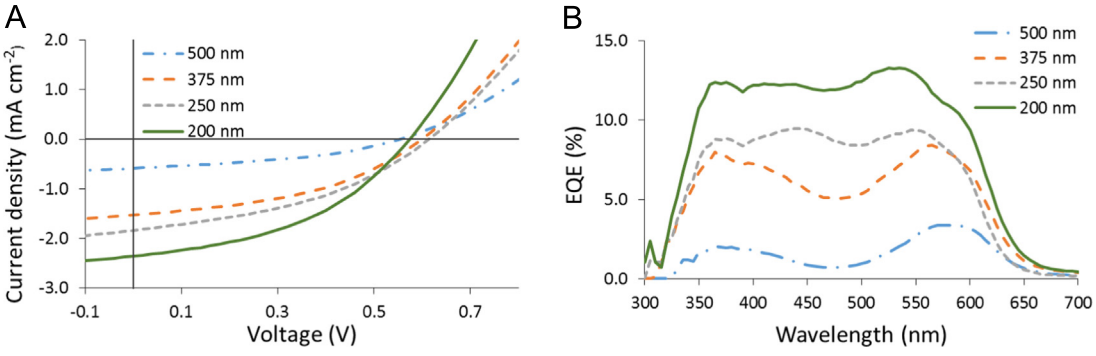

C

Active layer thickness	V_{OC} (V)	J_{SC} (mA cm^2)	FF (%)	PCE (%)
500 nm	0.57(0.06)	-0.52(0.06)	39.2 (0.16)	0.12(0.01)
375 nm	0.59(0.00)	-1.25(0.24)	43.3 (1.8)	0.32 (0.05)
250 nm	0.61 (0.00)	-1.80(0.11)	37.3(3.5)	0.41 (0.06)
200 nm	0.58(0.02)	-2.20(0.22)	42.7(0.38)	0.55 (0.04)

Fig. 3. (A) *I–V* curves of devices prepared with active layer thicknesses of 200, 250, 375, and 500 nm showing an increase in short circuit current with reducing layer thickness. (B) EQE curves of the devices in A. (C) Average device characteristics for devices with variation in active layer thickness.

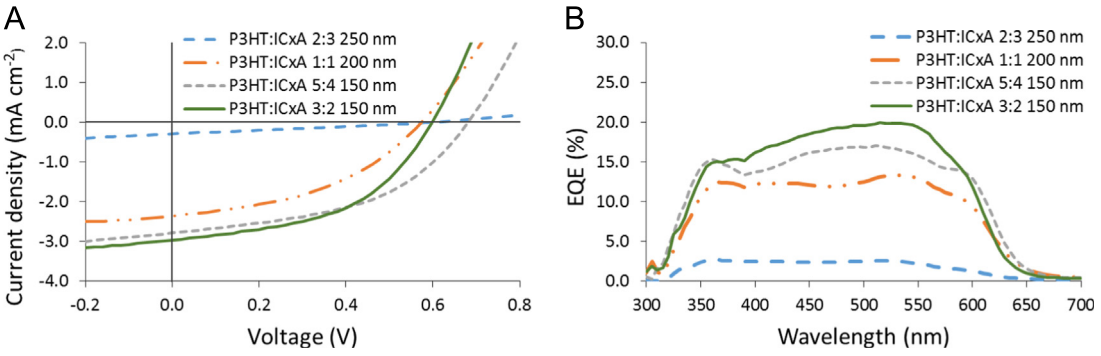

C

Ratio P3HT:ICxA	V_{OC} (V)	J_{SC} (mA cm^2)	FF (%)	PCE (%)
2:3	0.48	-0.30	27	0.048
1:1	0.58(0.02)	-2.20(0.22)	42.7 (0.38)	0.55(0.04)
5:4	0.68 (0.02)	-2.80(0.11)	46.7(0.32)	0.88 (0.01)
3:2	0.61(0.02)	-2.72(0.35)	49.0 (0.94)	0.81(0.07)

Fig. 4. (A) *I–V* curves of devices prepared with active layer ratios of 2:3, 1:1, 5:4 and 3:2 showing an increase in short circuit current and FF with an increased P3HT ratio. (B) EQE curves of the devices in A. (C) Average device characteristics for devices with variation in active layer component ratio except for 2:3 where only hero is displayed due to critical failure during switching.

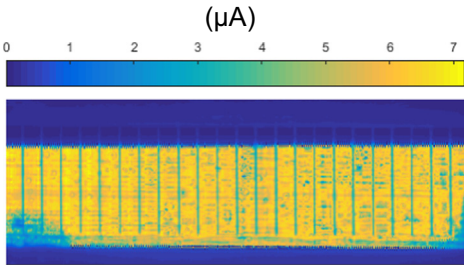

Fig. 5. LBIC image of an encapsulated device, yellow illustrates areas with high electron generation and extraction and blue illustrates areas with reduced or no current generation or extraction. The LBIC image shows the shadow from the grid lines in the front electrode and horizontal lines with reduced current generation. The areas with reduced current generation in the bottom corners are due to poor encapsulation. (For interpretation of the references to colour in this figure legend, the reader is referred to the web version of this article.)

which there is reduced or no photocurrent extraction (illustrated by the blueish areas within the yellow area). These features can also be seen in Fig. 2D as a colour variation in the AZO layer and arise from imperfections occurring during drying of the AZO layer. Further optimization of the AZO coating is currently underway to improve film quality.

To date, the requirements of all-solution processed R2R printed OSCs has driven the development of inverted geometry devices [38,39]. Moreover, the fact that the evaporation of metal cathodes is not readily R2R scalable, coupled with previous work indicating that sputtering can induce defect damage in active layer films [40] has meant that R2R printed normal geometry OSC architectures have not been widely explored. The results presented here show that with a judicious choice of ETL, sputtered cathodes can be readily fabricated resulting in all-R2R processed normal architecture solar cells. This development allows the application of R2R processed devices into new areas that are currently only being explored by small scale OSC devices, such as semi-transparent coatings, where the ability to sputter coat a transparent cathode is advantageous [41].

3. Conclusion

We have demonstrated a successful pathway for the preparation of organic solar cells in a normal geometry using an entirely roll-to-roll process that is compatible with large scale manufacture. The initial approach to prepare solar cells without an electron transport layer produced devices with poor solar cell characteristics. The incorporation of an aluminium doped zinc oxide layer produced devices which exhibit J-shaped *I–V* curves and improved current extraction. Optimizing the AZO layer for film quality and film thickness, an efficiency of 0.12% was achieved. The devices were further optimized by varying the active layer. Firstly, the film thickness was reduced from 500 nm to 200 nm, which increased the short circuit current from 0.55 to 2.20 mA cm^{-2}. The ratio between P3HT and ICxA was then varied, with an increase of the ICxA ratio found to lower the device efficiency, whereas increasing the P3HT ratio increased the efficiency from 0.55% to 0.88% at an optimal donor:acceptor ratio of 5:4 of P3HT and ICxA, respectively. The inherent advantages of metallized back contacts have been shown along with, for the first time, a pathway to producing these normal geometry devices at scale.

4. Experimental

4.1. Materials

Materials were used as received unless otherwise stated. Polyethylene terephthalate (PET) had a thickness of 75 μm and was purchased from Multapex. Poly(3,4-ethylenedioxy-thiophene):poly (styrenesulfonate) (PEDOT:PSS) Clevios PH1000 and HTL Solar was purchased from Heraeus. Silver ink (PFI-722) was purchased from Novacentrix. Poly(3-hexylthiophene) (P3HT) was synthesized in house according to literature and had an estimated molecular weight of 40 kDA. ICxA was synthesized in house according to literature [42]. Zinc acetate and basic aluminium acetate were purchased from Sigma-Aldrich. Aluminium doped zinc oxide (AZO) was prepared in methanol according to literature [43].

4.2. Ink formulation and deposition

Coating and printing were conducted on 30 cm width PET substrate on a Solar-1 coating line from Grafisk Maskinfabrik using a slot-die head developed at DTU Energy Conversion having a 50 mL ink dead volume to ensure uniform inking to all 13 stripes each having a width of 13 mm.

4.3. Charge collecting silver grid

Silver ink was R2R printed on to pre-stretch (heat treated at 140 °C for 2 min) PET using a patterned photopolymer flexo plate and 1.5 $cm^3\ m^{-2}$ anilox roller. The conductive silver grid pattern was printed as silver fingers with a length of 11 mm and a width of 100 μm connected to a busbar with a distance between fingers of 2 mm at 20 $m\ min^{-1}$ and annealed in an inline oven (4 m in length) at 140 °C for a dry thickness of approximately 200 nm.

4.4. PEDOT:PSS electrode

1 L of Clevios PH1000 was mixed with 265 mL of isopropanol, and 65 mL of dimethyl sulfoxide. The mixture was treated with an ultrasonic booster horn (650 W) for 2 × 30 s, after which 1.3 g of Zonyl® fluorosurfactant was added to the suspension and it was left to stir for 20 min prior to use. The PEDOT:PSS ink was slot-die coated with a web-speed of 1 $m\ min^{-1}$ and a wet thickness of 47 μm resulting in an approximately 200 nm thick film with a drying temperature of 140 °C.

4.5. HTL solar

HTL solar was mixed with IPA in a 1:2 ratio and treated with ultrasound (240 W) for 2 × 30 s prior to usage. HTL solar was slot-die coated with a web-speed of 1.5 $m\ min^{-1}$ with 4 m of ovens at 140 °C at a wet thickness of 16 μm.

4.6. Active layer

P3HT and ICxA were dissolved in a 90:10 mixture of chlorobenzene and chloroform, respectively, the solid concentration was between 22 and 30 $mg\ mL^{-1}$ to ensure a sufficient wet thickness during ink deposition. The active layer was deposited by slot-die coating with ovens temperature at 140 °C with a web-speed of 1.5 $m\ min^{-1}$ and the wet thickness of the coated film was between 9 and 21 μm in order to obtain theoretical dry thicknesses of 150–500 nm using estimated densities 1.1 and 1.5 for P3HT and ICxA, respectively.

4.7. Aluminium doped zinc oxide

Aluminium doped zinc oxide (AZO) was prepared in methanol according to literature [43]. The ink was slot-die coated on top of active layer at 140 °C with limited success. A better compatibility between the surface of the active layer and the ink was obtained via prewetting the surface of the active layer with isopropanol. A further improvement of film quality was finally obtained by prewetting with isopropanol and by addition of isopropanol to the AZO ink with a ratio of 65:35 of AZO ink and isopropanol, respectively. Deposition of AZO was conducted at 1 $m\ min^{-1}$ with a wet thickness of 5 μm and a drying temperature at 140 °C and further cured for 10 min at 140 °C as described in literature [43] by passing through 4 m of ovens at 0.4 $m\ min^{-1}$ resulting a film thickness of approximately 50 nm.

4.8. Sputtering

Sputter coating of aluminium cathodes was performed using custom-built R2R sputter coater capable of handling web width of 30 cm (Semicore Equipment, Inc.) further description can be found in [15]. The system is comprised of two terminal 7 cm spindles which besides unwinding and rewinding also ensures web-tension as the web travels around a water-cooled 22.9 cm drum. The sputtering chamber is evacuated to low vacuum (0.1 mTorr) with a Trivac D40B-D65B roughing pump (Oerlikon Leybold Vacuum) and then further evacuated to a high vacuum base pressure (10^{-6} Torr) using a water-chilled Cryo-Torr pump (Helix Technologies). Sputtering was performed in an argon plasma created by a direct current (DC) magnetron; with power supplied to the 35.6 × 10.1 cm^2 aluminium targets (Angstrom Sciences, Inc.) using separate 6 kW Pinnacle DC power sources (Advanced Energy Industries, Inc.) Sputtered cathodes for all OPV films in this study were subsequently conducted on a continuously moving substrate with a speed allowing for a deposition time of 42 s at a sputtering base pressure of 5×10^{-6} Torr, a process pressure of 2 mTorr, and a target power of 1.5 kW (power density=4.15 W cm^{-2}) yielding an aluminium thickness of approximately 100 nm. OPV films were for small samples (less than 10 m) roll-to-roll sputtered through a shadow mask applied to the samples with high temperature resistant tape.

4.9. Switching and encapsulation

Switching is an electrical activation of device prepared with PH1000 as described in literature [44]. Switching is conducted by subjecting the device to reverse bias in short pulses using an adjustable power supply with a current of 1 A and a voltage starting at 3 V. The reverse bias magnitude was subsequently increased in 2–3 V steps up to a maximum value of 20 V, which increased the resistance through the device from 2 Ω to 6–10 kΩ as a possible consequence of shunt burning and de-doping of PEDOT:PSS [44]. During the switching procedure critical failure (Fig. 6) can occur either as a consequence of coating errors or too short distance between the top and bottom electrode.

Fig. 6. The picture illustrates critical failure of devices during switching seen as burn and/or melted areas of the organic solar cell.

Devices were encapsulated between two pieces of microscope glass using a UV curable epoxy (Dymax SC 3220-gel) as adhesive and copper tape to ensure contact with the metal electrodes.

4.10. I–V measurement

Current density–voltage (*J–V*) measurements were performed using a Newport Class AAA solar simulator with an AM 1.5 spectrum filter on devices with a typical area of 4 cm^2 (8×50 mm^2). The light intensity was calibrated to 100 mW cm^{-2} using a silicon reference solar cell (FHG-ISE). *J–V* data was recorded in the dark and under illumination using a Keithley 2400 source metre. Data presented is averaged over 3–5 devices unless stated otherwise.

4.11. External quantum efficiency

External quantum efficiency (EQE) measurements were recorded by illuminating the devices with a tungsten halogen lamp passed through an Oriel Cornerstone 130 monochromator. An Ithaco Dynatrac 395 analogue lock-in amplifier and Thorlabs PDA55 silicon diode were employed to collect the reference signal, and a Stanford Research Systems SR830 DSP digitizing lock-in amplifier was employed to measure the device current.

4.12. Laser-beam induced current

Laser-beam induced current (LBIC) measurements were conducted using a custom-built setup as previously described [45]. Briefly, an electronically modulated laser diode (405 nm) is pigtailed into a single-mode optical fibre. The optical fibre is coupled into an assembly containing collimating and focussing lenses providing control over the spot radius down to 3.3 µm. For this study, a spot size of 100 µm was chosen, at which the photocurrent responds linearly with light intensity. The solar cell was mounted on 2 orthogonal computer-controlled translation stages. The short-circuit current of the solar cell was converted to a voltage using a current-to-voltage preamplifier (Stanford Research, SR570) before being detected using a lock-in amplifier (Stanford Research, SR830).

Acknowledgements

The work was performed in part at the Materials node of the Australian National Fabrication Facility, a company established under the National Collaborative Research Infrastructure Strategy to provide nano- and microfabrication facilities for Australia's researchers.

References

[1] G. Dennler, M.C. Scharber, C.J. Brabec, Polymer-fullerene bulk-heterojunction solar cells, Adv. Mater. 21 (2009) 1323–1338.
[2] C.J.M. Emmott, A. Urbina, J. Nelson, Environmental and economic assessment of ITO-free electrodes for organic solar cells, Sol. Energy Mater. Sol. Cells 97 (2012) 14–21.
[3] N. Espinosa, M. Hösel, D. Angmo, F.C. Krebs, Solar cells with one-day energy payback for the factories of the future, Energy Environ. Sci. 5 (2012) 5117–5132.
[4] F.C. Krebs, N. Espinosa, M. Hösel, R.R. Søndergaard, M. Jørgensen, 25th anniversary article: rise to power-OPV-based solar parks, Adv. Mater. 26 (2014) 29–39.
[5] M.A. Green, K. Emery, Y. Hishikawa, W. Warta, E.D. Dunlop, Solar cell efficiency tables (version 45), Prog. Photovolt. Res. Appl. 23 (2015) 1–9.
[6] M. Jørgensen, J.E. Carlé, R.R. Søndergaard, M. Lauritzen, N.A. Dagnæs-Hansen, S.L. Byskov, et al., The state of organic solar cells—a meta analysis, Sol. Energy Mater. Sol. Cells 119 (2013) 84–93.
[7] R. Søndergaard, M. Hösel, D. Angmo, T.T. Larsen-olsen, F.C. Krebs, Roll-to-roll fabrication of polymer solar cells as the performance in terms of power conversion efficiency and operational, Mater. Today 15 (2012) 36–49.
[8] R.R. Søndergaard, M. Hösel, F.C. Krebs, Roll-to-roll fabrication of large area functional organic materials, J. Polym. Sci. Part B: Polym. Phys. 51 (2013) 16–34.
[9] M. Hösel, R.R. Søndergaard, M. Jørgensen, F.C. Krebs, Fast inline roll-to-roll printing for indium-tin-oxide-free polymer solar cells using automatic registration, Energy Technol. 1 (2013) 102–107.
[10] J.-S. Yu, I. Kim, J.-S. Kim, J. Jo, T.T. Larsen-Olsen, R.R. Søndergaard, et al., Silver front electrode grids for ITO-free all printed polymer solar cells with embedded and raised topographies, prepared by thermal imprint, flexographic and inkjet roll-to-roll processes, Nanoscale 4 (2012) 6032–6040.
[11] F.C. Krebs, M. Hösel, M. Corazza, B. Roth, M.V. Madsen, S.A. Gevorgyan, et al., Freely available OPV—the fast way to progress, Energy Technol. 1 (2013) 378–381.
[12] T.T. Larsen-Olsen, T.R. Andersen, B. Andreasen, A.P.L. Böttiger, E. Bundgaard, K. Norrman, et al., Roll-to-roll processed polymer tandem solar cells partially processed from water, Sol. Energy Mater. Sol. Cells 97 (2011) 43–49.
[13] T.R. Andersen, H.F. Dam, M. Hösel, M. Helgesen, J.E. Carle, T.T. Larsen-Olsen, et al., Scalable, ambient atmosphere roll-to-roll manufacture of encapsulated large area, flexible organic tandem solar cell modules, Energy Environ. Sci. 7 (2014) 2925–2933.
[14] H.F. Dam, T.R. Andersen, M.V. Madsen, T.K. Mortensen, M.F. Pedersen, U. Nielsen, et al., Roll and roll-to-roll process scaling through development of a compact flexo unit for printing of back electrodes, Sol. Energy Mater. Sol. Cells 140 (2015) 187–192.
[15] M. Griffith, N. Cooling, B. Vaughan, D. Elkington, A. Hart, A. Lyons, et al., Combining printing, coating and vacuum deposition on the roll-to-roll scale: a hybrid organic photovoltaics fabrication, selected topics in quantum electronics, IEEE J. Sel. Top. Quantum Electron. 22 (2016) 4100614.
[16] L. Blankenburg, K. Schultheis, H. Schache, S. Sensfuss, M. Schrödner, Reel-to-reel wet coating as an efficient up-scaling technique for the production of bulk-heterojunction polymer solar cells, Sol. Energy Mater. Sol. Cells 93 (2009) 476–483.
[17] M. Schrödner, S. Sensfuss, H. Schache, K. Schultheis, T. Welzel, K. Heinemann, et al., Reel-to-reel wet coating by variation of solvents and compounds of photoactive inks for polymer solar cell production, Sol. Energy Mater. Sol. Cells 107 (2012) 283–291.
[18] Y. Galagan, I.G. de Vries, A.P. Langen, R. Andriessen, W.J.H. Verhees, S. C. Veenstra, et al., Technology development for roll-to-roll production of organic photovoltaics, Chem. Eng. Process.: Process Intensif. 50 (2011) 454–461.
[19] M.J. Griffith, N.A. Cooling, B. Vaughan, K.M. O'Donnell, M.F. Al-Mudhaffer, A. Al-Ahmad, et al., Roll-to-roll sputter coating of aluminum cathodes for large-scale fabrication of organic photovoltaic devices, Energy Technol. 3 (2015) 428–436.
[20] M.T. Lloyd, D.C. Olson, P. Lu, E. Fang, D.L. Moore, M.S. White, et al., Impact of contact evolution on the shelf life of organic solar cells, J. Mater. Chem. 19 (2009) 7638.
[21] F.C. Krebs, S.A. Gevorgyan, J. Alstrup, A roll-to-roll process to flexible polymer solar cells: model studies, manufacture and operational stability studies, J. Mater. Chem. 19 (2009) 5442.
[22] S. Albrecht, S. Schäfer, I. Lange, S. Yilmaz, I. Dumsch, S. Allard, et al., Light management in PCPDTBT:PC70BM solar cells: a comparison of standard and inverted device structures, Org. Electron. 13 (2012) 615–622.
[23] F.C. Krebs, M. Jørgensen, 2D characterization of OPV from single and tandem cells to fully roll-to-roll processed modules with and without electrical contact, Adv. Opt. Mater. 2 (2014) 465–477.
[24] T.R. Andersen, H.F. Dam, B. Andreasen, M. Hösel, M.V. Madsen, S. A. Gevorgyan, et al., A rational method for developing and testing stable flexible indium- and vacuum-free multilayer tandem polymer solar cells comprising up to twelve roll processed layers, Sol. Energy Mater. Sol. Cells 120 (2013) 735–743.
[25] C.J. Traverse, M. Young, S. Wagner, P. Zhang, P. Askeland, M.C. Barr, et al., Efficient zinc sulfide cathode layers for organic photovoltaic applications via n-type doping, J. Appl. Phys. 115 (2014) 194505.
[26] H. Fujimoto, T. Miyayama, N. Sanada, C. Adachi, Plasma-tolerant structure for organic light-emitting diodes with aluminum cathodes fabricated by DC magnetron sputtering: using a Li-doped electron transport layer, Org. Electron. 14 (2013) 2994–2999.
[27] L.S. Liao, L.S. Hung, W.C. Chan, X.M. Ding, T.K. Sham, I. Bello, et al., Ion-beam-induced surface damages on tris-(8-hydroxyquinoline) aluminum, Appl. Phys. Lett. 75 (1999) 1619.
[28] M. Jørgensen, K. Norrman, S.A. Gevorgyan, T. Tromholt, B. Andreasen, F. C. Krebs, Stability of polymer solar cells, Adv. Mater. 24 (2012) 580–612.
[29] N.K. Zawacka, T.R. Andersen, J.W. Andreasen, L.H. Rossander, H.F. Dam, M. Jørgensen, et al., The influence of additives on the morphology and stability of roll-to-roll processed polymer solar cells studied through ex situ and in situ X-ray scattering, J. Mater. Chem. A 2 (2014) 18644–18654.
[30] G.F.A. Dibb, M.-A. Muth, T. Kirchartz, S. Engmann, H. Hoppe, G. Gobsch, et al., Influence of doping on charge carrier collection in normal and inverted geometry polymer:fullerene solar cells, Sci. Rep. 3 (2013) 1–7.
[31] T.M. Clarke, C. Lungenschmied, J. Peet, N. Drolet, A.J. Mozer, A comparison of five experimental techniques to measure charge carrier lifetime in polymer/fullerene solar cells, Adv. Energy Mater. 5 (2015) 1401345.

[32] F. Laquai, D. Andrienko, R. Mauer, P.W.M. Blom, Charge carrier transport and photogeneration in P3HT:PCBM photovoltaic blends, Macromol. Rapid Commun. 36 (2015) 1001–1025.
[33] C.R. McNeill, Morphology of all-polymer solar cells, Energy Environ. Sci. 5 (2012) 5653–5667.
[34] J. Ajuria, I. Etxebarria, W. Cambarau, U. Mu, J.C. Jimeno, R. Pacios, Inverted ITO-free organic solar cells based on p and n semiconducting oxides. New designs for integration in tandem cells, top or bottom detecting devices, and photovoltaic windows, Energy Environ. Sci. 4 (2011) 453–458.
[35] D. Angmo, M. Bjerring, N.C. Nielsen, B.C. Thompson, F.C. Krebs, Fullerene alloy formation and the benefits for efficient printing of ternary blend organic solar cells, J. Mater. Chem. C 3 (2015) 5541–5548.
[36] L.H. Slooff, S.C. Veenstra, J.M. Kroon, W. Verhees, L.J.A. Koster, Y. Galagan, Describing the light intensity dependence of polymer:fullerene solar cells using an adapted Shockley diode model, Phys. Chem. Chem. Phys. 16 (2014) 5732–5738.
[37] J.E. Carlé, T.R. Andersen, M. Helgesen, E. Bundgaard, M. Jørgensen, F.C. Krebs, A laboratory scale approach to polymer solar cells using one coating/printing machine, flexible substrates, no ITO, no vacuum and no spincoating, Sol. Energy Mater. Sol. Cells 108 (2013) 126–128.
[38] F.C. Krebs, All solution roll-to-roll processed polymer solar cells free from indium-tin-oxide and vacuum coating steps, Org. Electron. 10 (2009) 761–768.
[39] F.C. Krebs, R. Søndergaard, M. Jørgensen, Printed metal back electrodes for R2R fabricated polymer solar cells studied using the LBIC technique, Sol. Energy Mater. Sol. Cells 95 (2011) 1348–1353.
[40] E. Ahlswede, J. Hanisch, M. Powalla, Influence of cathode sputter deposition on organic solar cells, Appl. Phys. Lett. 90 (2007) 063513.
[41] A. Colsmann, A. Puetz, A. Bauer, J. Hanisch, E. Ahlswede, U. Lemmer, Efficient semi-transparent organic solar cells with good transparency color perception and rendering properties, Adv. Energy Mater. 1 (2011) 599–603.
[42] N.A. Cooling, E.F. Barnes, F. Almyahi, M.F. Al-Mudhaffer, A. Al-Ahmad, B. Vaughan, et al., A low-cost mixed fullerene acceptor blend for printed electronics, J. Mater. Chem. A (resubmitted).
[43] J. Alstrup, M. Jørgensen, A.J. Medford, F.C. Krebs, Ultra fast and parsimonious materials screening for polymer solar cells using differentially pumped slot-die coating, ACS Appl. Mater. Interfaces 2 (2010) 2819–2827.
[44] T.T. Larsen-Olsen, R.R. Søndergaard, K. Norrman, M. Jørgensen, F.C. Krebs, All printed transparent electrodes through an electrical switching mechanism: a convincing alternative to indium-tin-oxide, silver and vacuum, Energy Environ. Sci. 5 (2012) 9467–9471.
[45] K. Feron, T.J. Nagle, L.J. Rozanski, B.B. Gong, C.J. Fell, Spatially resolved photocurrent measurements of organic solar cells: tracking water ingress at edges and pinholes, Sol. Energy Mater. Sol. Cells 109 (2013) 169–177.